Preparation and Characterization of TiO_2 Nanotubes Catalyst Support and Doped TiO_2 Nanotubes Arrays Sheet

Mohammed Ahmed Hussein Awad [*] Dr. Nabil A.N. Alkadasi [**]

Abstract

Highly ordered titanium oxide nanotubes (TONTs) were synthesized via the electrochemical anodic oxidation. The as-anodized TONTs were consequently annealed at 450 °C in ambient air and N_2 for 3hrs to obtain titanium oxide nanotubes annealed in air (TONTs-air) and titanium oxide nanotubes annealed in nitrogen (TONTs-N_2). V-doped and W-doped TiO_2 nanotubes arrays were synthesized via in *situ* doping method during anodization. All samples were annealed at 450 °C in ambient air and N_2 for 3hrs to obtain TONTs-air 10 mM Vanadium, TONTs-N_2 10 mM Vanadium, TONTs-air 10 mM Tungsten and TONTs-N_2 10 mM Tungsten.

The physicochemical characterization of the TONTs-arrays and doped-TONTs-arrays catalyst support were performed by X-ray diffraction (XRD) and scanning electron microscopy (SEM). The TONTs-arrays, doped-TONTs-arrays catalyst support were electrochemically characterized by typical current density-time (I-t) during anodization and also characterized in ferro-fericcyanide potassium system by cyclic voltammetry (CV) measurement. In addition, V-doped titanium oxide nanotubes arrays were photo chemically characterized and supporting electrolyte is 1M KOH.

Key words:

Titanium oxide nanotubes sheet, electrochemical anodization technique, vanadium, tungsten, doping, cyclic voltammetry, chronoamperometry

[*]Chemistry Department, Faculty of Applied Sciences, Thamar University
[**]Faculty of Engineering, Thamar University, and Al-Bayda'a University

1. Introduction

The semiconductor titania (TiO_2) is one of the best candidates for many applications, namely photocatalysis [1,2], implant materials [3], hydrogen sensing [4], solar cells [5] and other electrochemical devices. Thus is due to its high efficiency in UV light, low cost, chemical inertness, ecofriendly nature and photostability [6,7]. Titania (TiO_2) is the greatest extensively used photo catalyst for the purification of air, water, and additional environmental applications owing to its great photocatalytic activity, admirable chemical stability, comparatively low price, and its deficiency of any recognized toxicity.

Nanostructured TiO_2 semiconductors have great potential in photo electrochemical devices due to the large effective light harvesting interface area and wider band gap. Anodization of Ti is a simple way to prepare a well-ordered nanostructured TiO_2 in the form of vertically oriented titania nanotube arrays. When compared with unordered nanoparticles, nanotube arrays facilitate charge transport along the tube direction [8,9] while maintaining a high effective surface area. Titania nanotubes are thus suitable for a variety of applications such as sensors [10], water photoelectrolysis [11], photovoltaic devices [12], photocatalytic CO_2 reduction [13], supercapacitors [14], etc. The use of titania nanotubes as photoelectrode in photovoltaic devices has the potential to enhance the efficiency. Therefore, titania nanotube growth by anodization has been studied widely in literature [15,16] , in order to form a well-ordered tubular structure with controlled morphology, a balance between oxidation and field-assisted dissolution has to be maintained by adjusting electrolyte concentration, temperature [17], duration of anodization, ramp rate and the applied potential [16].

TiO_2 is regarded as the most attractive photo catalyst with excellent photocatalytic properties. However, it is only activated by UV light ($\lambda < 387$ nm) due to its large band gap of 3.2 eV.

Reduction/oxidation (redox) reactions of environmental attention are started on the TiO_2 surface with trapped electrons and holes after band-gap excitation. However, owing to its large band gap energy of ~3.2 eV (electronvolt), TiO_2 is useful only in the ultraviolet region of the solar spectroscopy. As a result, major

efforts have been made to improve modified TiO_2 which are energetic under visible-light ($\lambda > 400$ nm) irradiation. Numerous different approaches have been employed to extend photo activity into the visible region. They consist of:

(I) Doping with anions: such as nitrogen] 18-20], sulphur, iodine [21], and fluorine, etc.

(II) Metal cations doping [2]

(III) Functionalizing TiO_2 by photo-sensitizers that have the ability to absorb visible-illumination. The greatest vigorously followed approach has been to increase the photoactive wavelength range and to improve the photo catalytic activity under UV radiation using metal doped TiO_2 nanotubes.

Several metal ions have been examined as possible dopants ions such as Fe, V [22], Cr, Ni and K [22] and have been showed UV light photo catalytic activity. Furthermore, efforts have been made to increase the visible and UV light photo catalytic activity for TiO_2 using co-doping by means of two metal ions.

Ahmad et al. [23] reported that Sc and Nb co-doped TiO_2 nanoparticles are comparatively more photoactive for 2-chlorophenol degradation under visible-illumination than the particles doped with Sc or Nb only. Kato ND Kudo [24] reported that TiO_2 co-doped with Sb^{3+} and Cr^{3+} ions exhibited higher activity than TiO_2 doped only with Cr^{3+} ions alone for O_2 evolution due to the charge compensation attained with Sb^{5+} doping.

Nevertheless, there have been comparatively insufficient researches stated for twofold metal ion co-doping of TiO_2, whereas TiO_2 co-doped with two nonmetals (such as N with F, and N with S) with metal ions and nonmetals (such as Cr and N co-doping, Pt and N co-doping, V and N co-doping [25], and Bi and S co-doping) have been extensively examined.

In order to examine the double-doping efficiency by metal cations, co-doped TiO_2 with Pt^{4+} (or Pt^{2+}), Cr^{3+}، V^{3+}, and Ni^{2+} ions have been prepared and characterized their physicochemical properties and photo catalytic activities for the decolorizing and methylene blue (MB) degradation, the iodide oxidation to tri-iodide, and the oxidative degradation of phenol in aqueous solution under visible-light irradiation ($\lambda > 400$ nm) [24].

Later, Asahi et al. stated that it is possible to narrow the band-gap of titanium dioxide by N_2-doping [27].

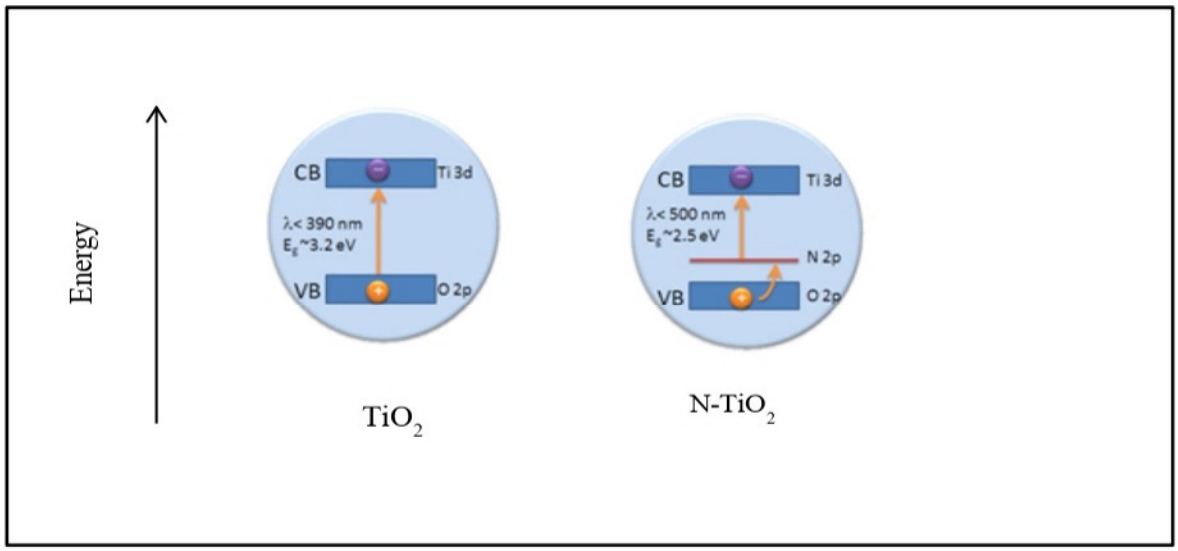

Fig.1: N-doping as clarified by *Nakamura* etal [26]. N_2-doping results in a mid-band gap energy level which diminishes the energy gap involved for charge separation.

2. Experimental

2.1 Materials:

Titanium foils (> 99.5% purity, Alfa Aesar, thickness: 0.25 mm). Hydrofluoric acid 40 % HF (A.Qualikemes Fine Chemicals,New Delhi.potassium chloride GRG KCl (WINLAB), 0.5 wt.% HF,potassium hexacyanoferrate (II) trihydrate $K_4[Fe(CN)_6].3H_2O$ (MERCK), potassium hexacyanoferrate(III) K_3 [Fe (CN) $_6$] (MERCK). All aqueous solutions were prepared by means of Milli-Q (Millipore, Inc.), high quality deionized (DI) water (resistance 18.2 MΩ cm).

The Chemicals used in the in situ doping method were as follows: Anhydrous ethanol 99.7-100 % V/V (from BDH Analar), ammonium meta vanadate NH_4VO_3 analytical reagent (from BDH Chemicals Ltd Poole England), and sodium tungstate dihydrate GR $Na_2WO_4.2H_2O$ (from MERCK).

2.2 Anodization process

High purity titanium sheets (>99.5% purity, Alfa Aesar, thickness: 0.25 mm) were degreased in an ultrasonic bath with isopropanol then acetone, washed in deionized water and dried in air at room temperature.

Highly ordered TONTs were synthesized via the electrochemical anodic oxidation. The titanium foils (>99.5% purity, Alfa Aesar, thickness: 0.25 mm) were anodized in an aqueous solution contains 0.5 wt. % HF by using a two-electrode polypropylene electrochemical cell which consists of Ti foil as the anode and Pt foil as the cathode at 20V for 20 min at room temperature with magnetic agitation. Then the samples were rinsed in deionized water and dried.

The as-anodized TONTs were consequently annealed at 450 °C in ambient air or N_2 for 3 hr using tubular furnace with heating and cooling rates of 5 °C min^{-1} to prompt anatase crystallization.

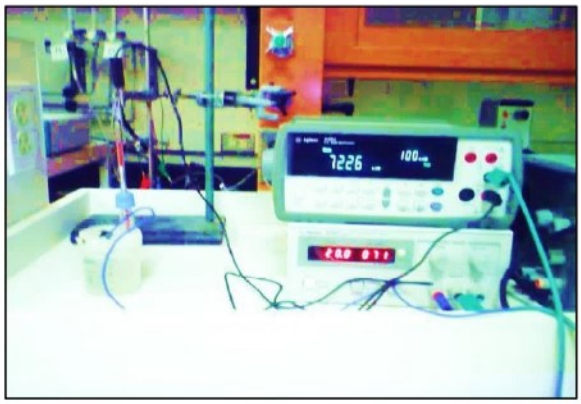

Fig. 2: Anodization process set up.

Electrochemical experiments were conducted by means of a direct current (dc) power supply (Agilent E3612 A 0-60V,0-0.5 A/0-120V , 0-0.25A DC power supply) and connected to (Agilent 34405A 5 ½ Digit multimeter). All were connected to computer and the program used is (Excel Inuilink for Multimeters Toolbar Addin).

2-3 In situ doping method during anodization

Anodization was conducted in 0.5 wt. % HF in which certain amount of the corresponding metal ions was added. Titanium foil functioned as anodic electrode and platinum electrode as the cathode. Anodization voltage was 20V. The metals-dopants were 10mM and 50mM vanadium (V), 10mM tungsten ($Na_2WO_4.2H_2O$ salt).

All experiments of anodization were carried out at room temperature using magnetic stirrer. After anodization, the titanium sheet surface color was yellowish and the samples were washed in deionized water and then dried. The as-anodized TiO_2 NTs were annealed in air and also in N_2 at 450°C for 3 h with a heating and cooling rate of 5 °C/min.

In this section, we proved successfully that in situ electrochemical doping method for TiO_2 nanotubes, which is the addition of different anion species in the electrolyte upon anodization nanotubes growth, is used to modify the conductivity properties of the material.

2.4 Physicochemical characterizations

(SEM; JSM-6380LA). Scanning Electron Microscopy (SEM) images were taken at magnification of 2000x, 10000x, 20000x, 50000x and 120000x to study the samples morphology.

X-ray diffraction (XRD) data were collected on a Model RIGAKU MINIFLEX 100 X-ray diffract meter, operating at tube voltage 40 kV and tube current 15 mA, using Cu(Kα) , intensity was 0-400 cps , range of 2θ(deg) was 5-80 degree i.e. wide angle. For chilar, the water flow rate was 3.7 L/min, scan rate either 5 °/min or 2 °/min. Monochromator is used.

2.5 Electrochemical measurements

We use the typical current density-time (I-t) characteristics of TONTs-as anodized at a constant potential of 20 V during the anodization process 20 min in the presence of 0.5 wt. % HF.

Cyclic Voltammetry (CV)

Cyclic voltammetry (CV) was conducted in a conventional three-electrode single-compartment Pyrex glass cell by using a computerized potentiostat/galvanostat (μAUTOLAB, TYPE III). The reference and auxiliary electrodes were standard calomel electrode (SCE) and pure Pt-foil, respectively. All potentials provided in the text are based on the SCE electrode only. The software program used in cyclic voltammetry measurements was NOVA 1.9.

2.6 Photo electrochemical measurements

The photoelectrochemical performance of the TONTs-N_2 and TONTs-N_2/ 10 mM Vanadium were evaluated using a three-electrode configuration with TONTs-N_2/ 10 mM Vanadium electrode, calomel electrode , and Pt as working, reference, and counter electrode, respectively. The supporting electrolyte used was 1 M KOH solution. All the potentials were referred to calomel electrode unless otherwise stated in this paper. The photocurrent was measured under an irradiation UV from Max-303 compact Xenon light source. The scan rate for the linear sweep voltammetry was 50 mV s^{-1}. The

photoresponse was evaluated under chopped light irradiation (light on/off cycles: 20 s) at a fixed electrode potential of 1.0 V.

The curves of the **I-t** and **V-t** are obtained using potentiostat/galvanostat. The software program used in cyclic voltammetry (CV) and chronoamperometry measurements under illumination (UV-Light) was EC-Lab.

3. Results and discussion

3.1 Preparation and Physicochemical Characterization of TiO_2 nanotubes (TONTs) catalyst support

The morphology and composition of the obtained oxide nanotubes were evaluated using SEM JSM-6380 LA equipped with an energy dispersive X-ray analyzer (EDX).Fig. 3 shows the SEM surface image (the top-view image) for TONTs-as anodized obtained under 20 V. TiO_2 nanotubes diameter is affected by the applied potential [28-30]. From the SEM image we can see the formation of highly packed array of pores.

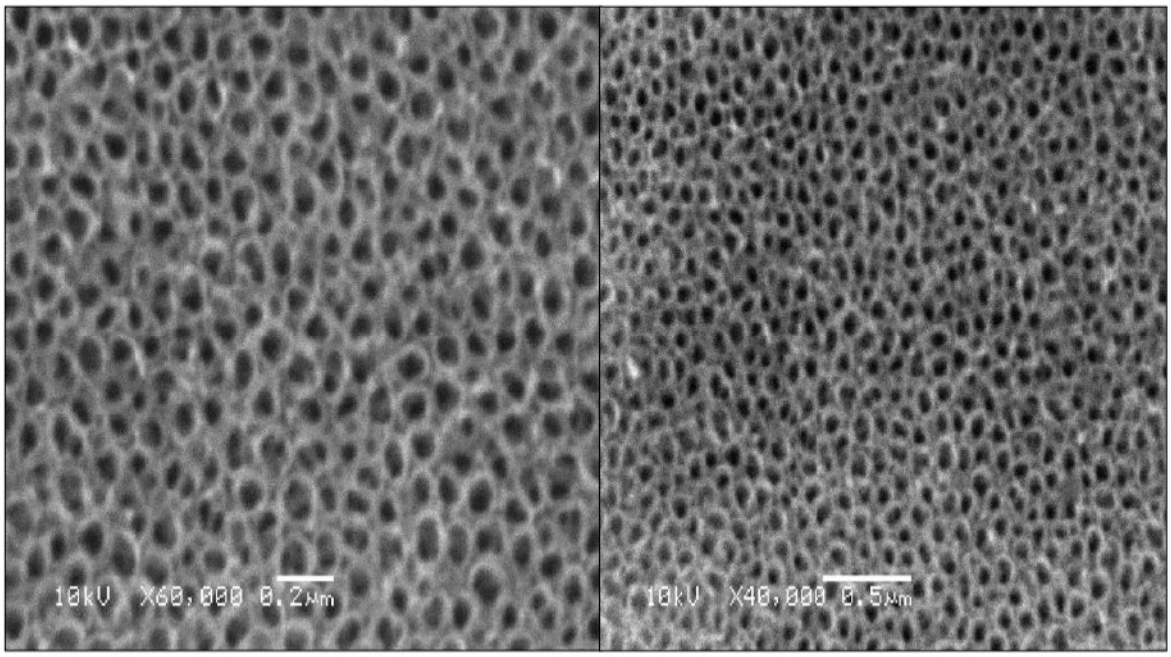

Fig.3: SEM image of TiO_2 nanotubes formed at 20V for 20 min, in 0.5 wt. % HF in DI water at different scales (0.2 µm and 0.5 µm).

Fig. 4 shows a comparison between XRD patterns of (a) titanium oxide nanotube sample after annealing at 450 °C, 3 hr in air besides (b) annealing in N_2 atmosphere. The XRD patterns show the presence of anatase and rutile phase mixture of titanium oxide. The major rutile orientation is the (101) plane and other planes, such as (200) and (202) are only existing in a minor amount. The XRD patterns showed the presence of

anatase phase planes (101) and (224) signifying the phase transition from amorphous to anatase crystal. It was reported that while heating at higher temperature than 450 °C annealed in nitrogen, it results the formation of rutile phase [31]. From Fig. 4 a and b, the XRD peaks at 2θ = ~ 38, ~ 43, ~54, ~ 72, ~ 78, and ~ 90 are originated from the Ti substrate. The XRD results obtained for the phase formation are in a good agreement with the literature data [32, 33]. The XRD of TONTs arrays annealed in N_2 at 450° C (Fig. 4 b) for 3 hr possess similar XRD patterns regardless of the annealing gas atmospheres.

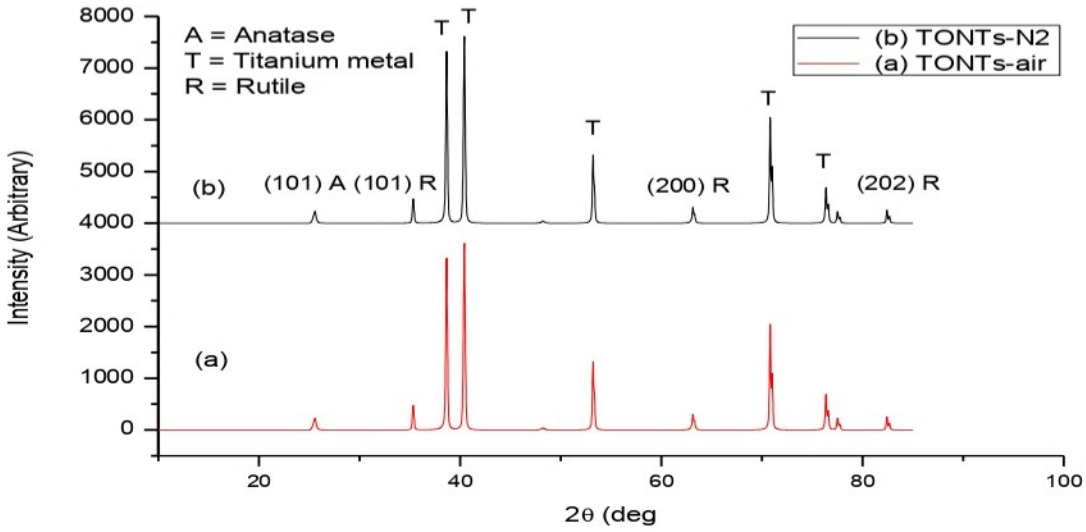

Fig. 4: Comparison of XRD shapes of nanotube samples after (a) annealed in air (b) annealed in N_2 at 450° C for 3 hr.

3.2 Electrochemical Characteristics of TiO_2 nanotubes

Fig. 5 displays the current time (I vs. t) curves recorded at the constant anodization voltage of 20 V in 0.5 wt. % HF titanium foil (area = 4.2 cm^2). In this case, at the beginning, the current decreases rapidly and reach the steady-state (where no change in current) within 800 seconds. However, in case of titanium foil (area = 4.2 cm^2) the current slightly change (increases to a maximum point then decreases slowly) before reaching the steady state as seen in Fig. 5 This I vs. t curve in good agreement with the mechanism described in literature [34] which is summarized below. The formation of the nanotubes is governed by competition between two processes, anodic oxide formation and chemical dissolution of the oxide as soluble fluoride complexes [34]**.** This is consistent with reported literatures [35-40]. The inset carton in Fig. 5 clarifies the pore formation process [41]. In part I, a barrier oxide layer formed, causing a current decay and in part II the surface is locally stimulated and pores start to grow randomly

which leads to the increase in current and pores growing. In stage (III), the individual pores start interfering with each other, competing for the obtainable current and then self-ordering under established steady-state conditions.

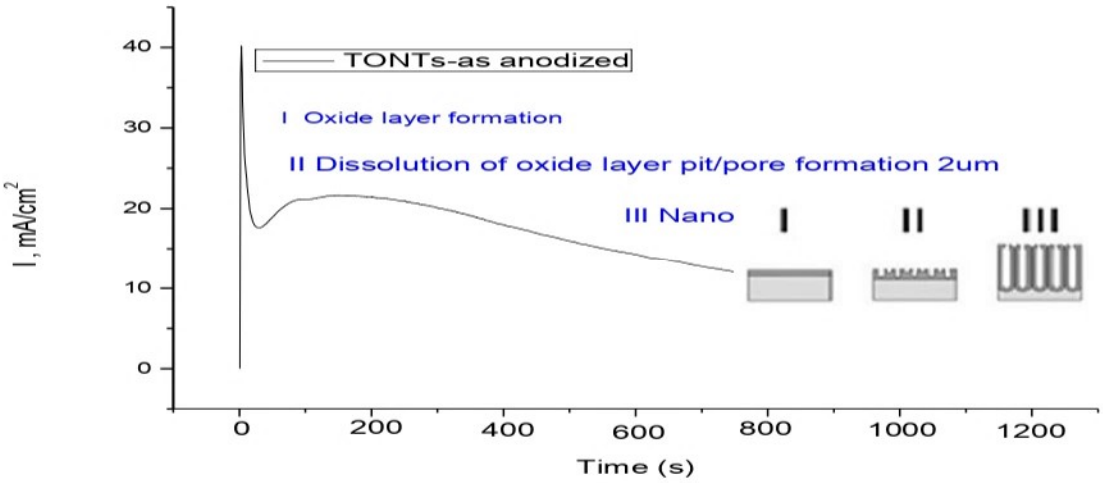

Fig. 5: Typical current density-time (I-t) characteristics of TONTs-as anodized at a constant potential of 20 V during the annodization process 20 min in the presence of 0.5 wt. % HF.

The inset carton shows the compact oxide (fluoride free) or porous/tubular metal oxide formation (containing fluoride) forms by different morphological phases(I–III).Therefore, type (I) indicates oxide layer formation, type (II) indicates dissolution of oxide layer pit/pore formation 2 μm, and type (III) indicates nanotubes growth.

The electrochemical properties of TiO_2 NTs electrodes annealed under different gases were investigated using cyclic voltammetry in 10mM $[Fe(CN)_6]^{-3/-4}$ + 0.5 M KCl electrolyte in a potential range from (− 0.5 V to 1V) vs. SCE at a scan rate of 50 mV/s.

Fig. 6 (a) shows the CVs of TONTs-as anodized, TONTs-air electrode and TONTs-N_2 respectively. The TONTs-as anodized, TONs-air and TONT-N_2 electrodes show an oxidation peaks at 0.53V, 0.72V and 0.46V and reduction peaks at -0.37V, -0.107V and -0.0166 V respectively. The reduction/oxidation peak separation ΔE_p was approximately 0.90V, 0.83 V, 0.48 V for TONTs as anodized, TONTs-air and TONTs-N_2 respectively.

This peak separation indicates that the reaction of $[Fe(CN)_6]^{-3/-4}$ at TONTs-N_2 shows better reversibility than on other electrodes [42]. The large peak separation is ascribed to the low electrical conductivity of the TONTs -air electrode [42, 43]. However, TONTs-N_2 shows the smallest peak separation among all studied electrode indicating on the conductivity improvement of TONTs by annealing in N_2.

In Fig. 6 the TONTs-N_2 electrode gives rise to larger ferri/ferrocyanide reduction peak currents than for the TONTs-as anodized and TONTs-air electrodes. This possibly reflects the greater surface area of the TiO_2 nanotubes annealed in N_2 and good conductivity. It may also be owing to the increased rate of diffusive mass transport of the ferri/ferrocyanide reactant to the nanotube surface (the latter being considered a supported nanoelectrode) [44]. In fact, the bulk oxide (BO) electrode displays only insignificant reactions at these anodic over voltages due to the blocking character that is an inherent characteristic for an n type semiconductor under anodic bias [45]. Annealing of TONT in nitrogen may enhance its conductivity through the substitution with oxygen in anatase phase [46, 50].

Several literatures have stated that the modification of the band gap of TiO_2 due to the Ti^{4+} reduction for instance; Macak selectively switched on the pore bottoms by reductive self-doping of TiO_2 nanotube with Ti^{3+} and established an adequate conductivity contrast to allow Cu deposition [47]. Guillemot proved that low temperature vacuum annealing could generate a controlled number of Ti^{3+} flaws [48]. Modification of electrical properties of oxides through thermal annealing under different gases is likewise well established in literature [49]. On the other hand, Fig. 6 b shows effect of scan rate for TONTs-N_2 electrode recorded at different scan rates for $[Fe(CN)_6]^{3-/4-}$ solution, Fig. 6 b shows an enhanced cathodic and anodic peak current that increases linearly with increasing scan rate, this behavior is characteristic of an electrochemical reaction controlled by a diffusion process.

Annealing under N_2 environment is probable to give rise to reduction of part of Ti^{4+} cations to lower valence state. Simultaneously, defects, for instance the oxygen vacancies, can be created in the TiO_2 structure owing to a partial oxygen loss [50]. That in turn would modify the electron density and the electrical properties of the material.

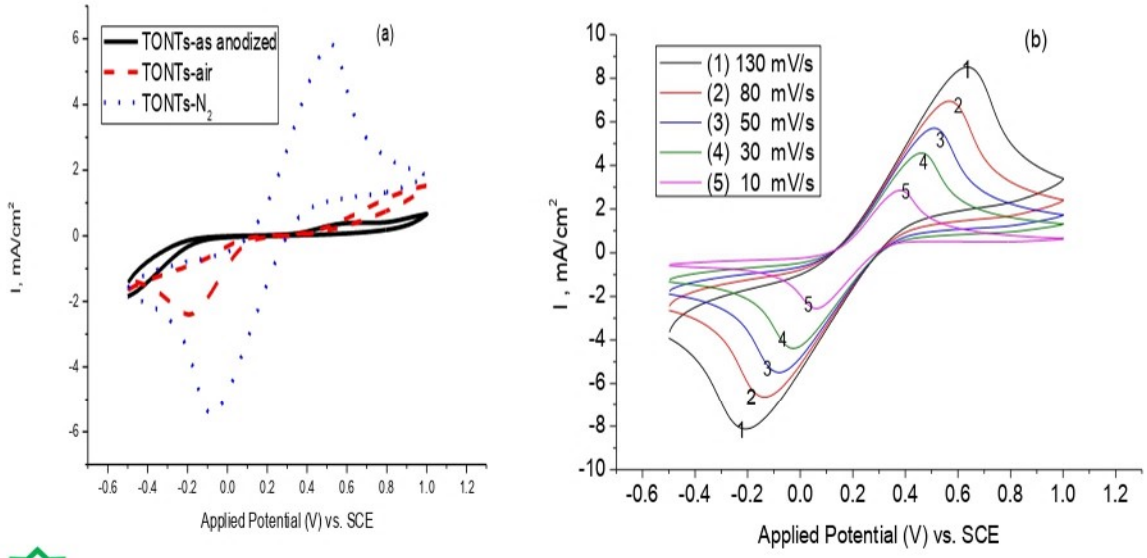

Fig. 6: CVs of 10mM K_4 [Fe (CN) $_6$] + K_3 [Fe (CN)$_6$] + 0.5 M KCl , scan rate 50 mVs^{-1} with (a) contains TONTs-as anodized, TONTs-air, TONTs-N_2 (b) effect of scan rate for TONTs-N_2 electrode in a potential range from (− 0.5 V to 1V) vs. SCE.

Table 1: Oxidation peaks, reduction peaks and reduction/oxidation peaks separation (ΔE) for TONTs-as anodized, TONTs-air and TONTs-N_2.

Electrode	Oxidation peaks potential (V)	Reduction peaks potential (V)	ΔE (V)
TONTs-as anodized	0.53	- 0.37	0.9
TONTs-air	0.72	- 0.107	0.83
TONTs-N_2	0.46	- 0.0166	0.48

Table 1 shows that the TONTs-N_2 support has lowest peak potentials of oxidation and highest reduction and lowest separation in contrast to TONTs-air and TONTs-as anodized indicates that TONTs-N_2 support has high conductivity.

In addition, the electrochemical properties of TiO_2 NTs annealed under different gases and 0.07 cm^2 glassy carbon electrodes were investigated by means of cyclic voltammetry in 10mM [Fe (CN) $_6$]$^{3-/4-}$ + 0.5 M KCl electrolyte in a potential range from (− 0.2 V to 0.5V) vs. SCE at a scan rate of 50 mV/s. Fig. 7 which shows the CVs of TONTs-as anodized, TONTs-air electrode, TONTs-N_2, and 0.07 cm^2 glassy carbon electrodes. The TONTs-N_2 and 0.07 cm^2 glassy carbon electrodes show an oxidation peaks at 0.32V and 0.22V and reduction peaks at 0.05V and 0.15V respectively.

The reduction/oxidation peak separation ΔE_p was approximately 0.27V for TONTs-N_2 and 0.07 cm^2 glassy carbon respectively. The anodic current density was approximately 2.5mA/cm^2 and 2.9mA/cm^2 . In addition the cathodic current density was approximately 2.4mA/cm^2 and 2.8mA/cm^2 for TONTs-N_2 and 0.07 cm^2 glassy carbon electrodes respectively and these values indicates that 0.07 cm^2 glassy carbon exhibit high electrical conductivity in contrast with other electrodes.TONTs-N_2 show also electrical conductivity close to that of 0.07 cm^2 glassy carbon but higher than that of TONTs-as anodized and TONTs-air electrodes.

This was evidence that the TONTs-N_2 have high electocatalytic activity but little less conductivity than that of 0.07 cm^2 glassy carbon electrode. Furthermore, the ratio of

peak anodic current density to the peak cathodic current density (I_{pa}/ I_{pc}) is approximately 1.04 and 1.04 for TONTs-N_2 and 0.07 cm^2 glassy carbon electrodes respectively, i.e. equals to 1(close to unity) indicating on quasi-reversible process.

It was reported in many literatures that the reversible process has reduction/oxidation peak separation smaller than 59/n mV, and n is the number of electrons . The ratio I_{pa}/ I_{pc} is also close to unity (I_{pa}/ I_{pc} = 1) [51,52]. Likewise, the quasi-reversible process has reduction/oxidation peak separation greater than 59/n mV.

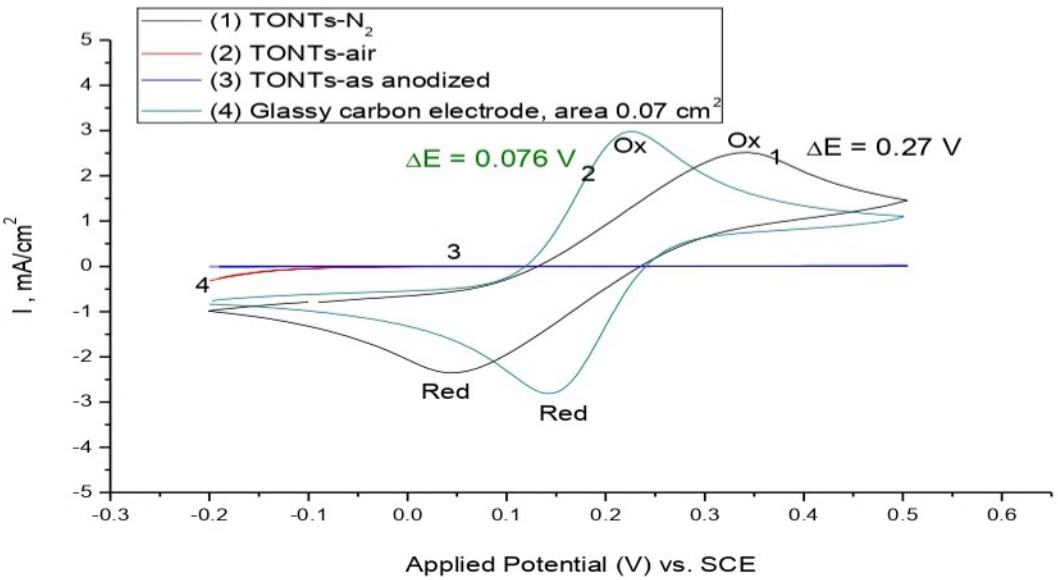

Fig. 7: CVs of 10mM [K_4 Fe(CN)$_6$] + 0.5 M KCl , scan rate 50 mV/s, at 20 V for 20 min contains TONTs-N_2 in 450 °C , time 3h, TONTs-air in 450 °C time 3h ,TONTs-as anodized, in contrast with glassy carbon electrode with area 0.07 cm^2 , window of potential range (-0.2V to 0.5V).

Table 2 shows the oxidation and reduction peaks of potentials and current density, and also separation of TONTs-N_2 and 0.07 cm^2 glassy carbon working electrode.

Table 2: Comparison between TiO_2 NTs annealed in N_2 and 0.07 cm^2 glassy carbon working electrode

Electrode	E_{pa} (V)	E_{pc} (V)	ΔE (V)	I_{pa} (mA/cm^2)	I_{pc} (mA/cm^2)	I_{pa}/ I_{pc}
TONTs-N_2	0.32	0.05	0.27	2.5	-2.4	1.04
Glassy carbon electrode with area 0.07 cm^2	0.22	0.15	0.07	2.9	- 2.8	1.04

3-3 Preparation and electrochemical characterization of V-doped and W-doped TiO_2 nanotubes arrays

In situ doping approach using vanadium and tungsten metals into titanium oxide nanotubes during anodization was carried out. Concentration of vanadium , and tungeston dopants metals was 10mM and the used electrolyte was 0.5 wt.% HF.

Fig. 8 shows the CVs of TONTs-N_2/10mM W, TONTs-N_2/10mM V and TONTs-N_2 respectively which were annealed in nitrogen gas at 450 °C for 3 hours. The TONTs-N_2/10mM W, TONTs-N_2/10mM Vanadium and TONTs-N_2 show an oxidation peaks at 0.757V, 0.447 V and 0.474V and reduction peaks at 0.501 V, 0.098 V and 0.098 V respectively. The reduction/oxidation peak separation ΔE_p was approximately 0.26 V, 0.35 V and 0.38 V for TONTs-N_2/10mM W, TONTs-N_2/10mM V and TONTs-N_2 respectively. In Fig. 6, Fig. 7 and Fig. 8, there is contradiction between the peak potentials and ΔE because of the electrode resistance, consumed quantity of fluoride during anodization, adsorbed nitrogen on TONTs substrate, and using of different potentials range (-0.5 V to 1V, -0.2V to 0.5 V, and -0.7 V to 1.7 V). The peak of separation indicates that the reaction of $[Fe(CN)_6]^{3-/4-}$ at TONTs-N_2 is reversible reaction than on other V and W doped TONT arrays electrodes. TONTs-N_2/10mM Tungsten shows the smallest separation peak of among all studied electrodes indicating high conductivity of TONTs doped by tungsten and annealed in N_2.The peak position for W-doped TONTs-N_2 electrode significantly shifted to positive due to the electrode is more resistant.

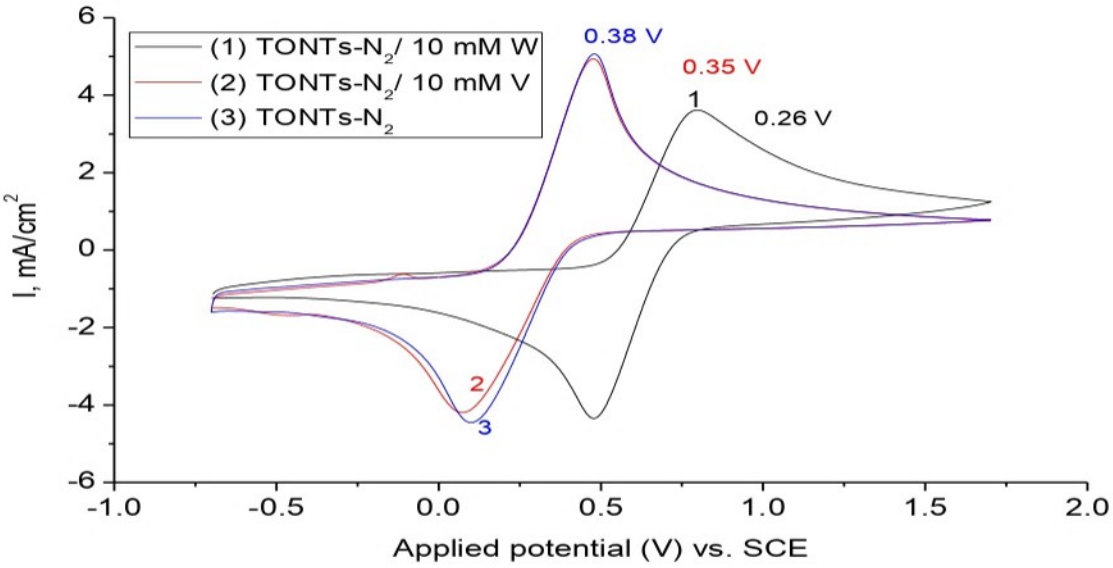

Fig. 8: CVs of 10mM $K_4(Fe(CN)_6)$ + 0.5 M KCl, scan rate was 50 mV/s with a TONTs-N_2, TONTs-N_2/10mM V, TONTs-N_2/10mM W, window of potential range (-0.7V to 1.7V).

In Fig. 9 it is clear that the reduction/oxidation peak separation ΔE_p was approximately 0.35 V, 0.39V and 0.38 V for TONTs-N_2/10mM V, TONTs-N_2/50mM Vanadium and TONTs-N_2 respectively. Fig. 9 shows the effect of vanadium concentration on separation and it is clear that there is no high effect on separation.

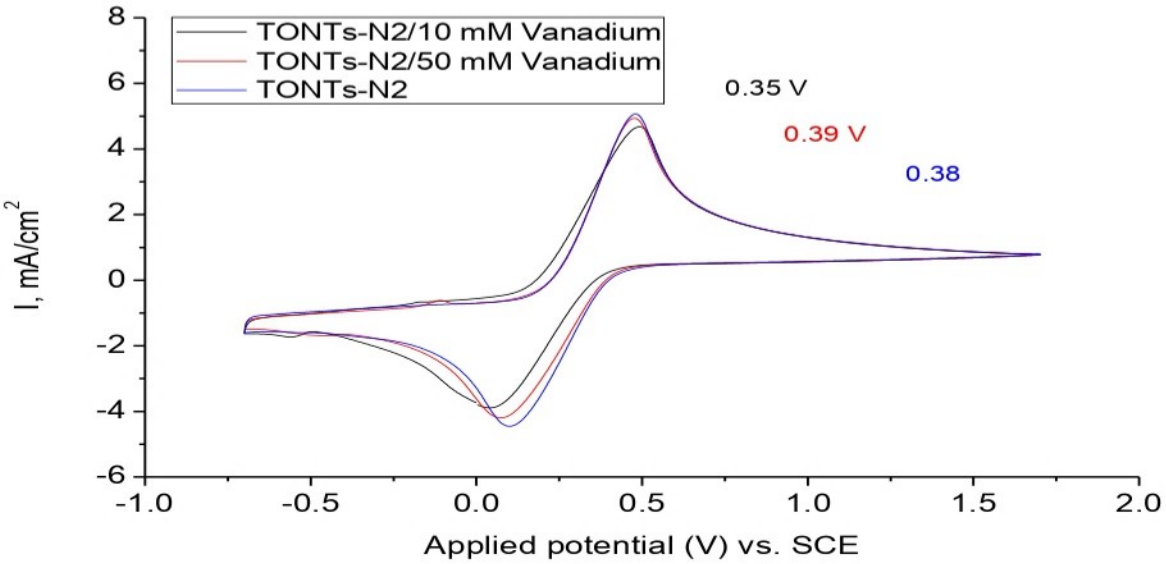

Fig. 9: CVs of 10mM $K_4(Fe(CN)_6)$ + 0.5 M KCl, at a scan rate 50 mV/s with a TONTs-N_2/10mM V dopant, TONTs-N_2/50mM V dopant, TONTs-N_2.

Fig. 10 shows the CVs of TONTs-N_2/ 10mM V, TONTs-air/ 10mM V, TONTs-N_2, and TONTs-air annealed at 450 °C for 3 hours respectively .The TONTs-N_2/ 10mM V, TONTs-air/ 10mM V, TONTs-N_2, show an oxidation peaks at 0.447V, 1.038V, and 0.474 V and reduction peaks at 0.098 V, -0.580V and 0.098 V respectively. The reduction/oxidation peak separation ΔE_p was approximately 0.35 V, 1.62V and 0.38 V for TONTs-N_2/10mM V, TONTs-air/10mM Vanadium and TONTs-N_2 respectively. Fig. 10 shows comparison between doping of 10mM vanadium on TONTs-N_2 and TONTs-air by in situ approach respectively. From Fig. 10 we conclude that TONTs-N_2 doped or undoped with Vanadium are the best electro catalysts in contrast with other electrodes which were annealed in air.

This indicates that the effect of V dopant on TONTs-N_2 is very little but the effect of V dopant on TONTs-air is very clear and high.

The anodic current density was approximately 4.7 mA/cm^2 and 2.4 and 4.6 mA/cm^2 . The cathodic current density was also approximately -4.1 mA/cm^2 , -2.4 mA/cm^2 and -4.2mA/cm^2 for TONTs-N_2/10mM V, TONTs-air /10mM V and TONTs-N_2 electrodes respectively. These values indicate that TONTs-N_2/10mM V exhibit high electrical conductivity in contrast with other electrodes and this was evidence that the TONTs-N_2/10mM V have high electrocatalytic activity. Furthermore, the ratio of peak anodic current density to the peak cathodic current density (I_{pa}/ I_{pc}) is approximately 1.14 ,1.00 and 1.12 for TONTs-N_2/10mM V, TONTs-air /10mM V and TONTs-N_2 electrodes respectively ,i.e. equals to 1 (close to unity)

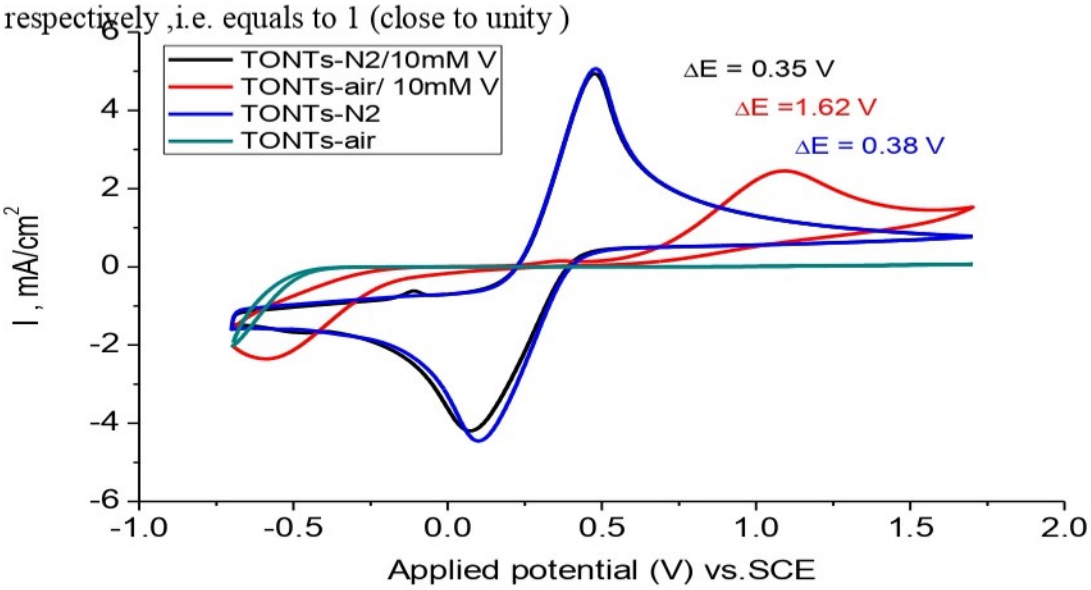

Fig. 10: CVs of TONTs-N_2, TONTs-N_2/10mM V, TONTs-air, and TONTs-air/ 10mM V, in ferro-fericcyanide system (10mM Ferro/ferric-cyanide + 0.5 M KCl) at a scan rate 50mV/s.

Table 3 shows the composition of an oxidation peaks, reduction peaks, reduction/oxidation peak separation ΔE_p, anodic peak current density $I_{p,a}$ (mA/cm^2), cathodic peak current density $I_{p,c}$ (mA/cm^2), the ratio of I_{pa}/ I_{pc} for TONTs-N_2,TONTs-N_2/10mM W ,TONTs-N_2/10mM V,TONTs-N_2/50mM V, and TONTs-air/10mM V respectively.

Table 3: Composition of the ΔE and I_{pa}/ I_{pc} for the V-doped and W-doped on TONTs-N_2 catalysts support.

Dopant	$E_{p,a}$ (V)	$E_{p,c}$ (V)	ΔE (V)	$I_{p,a}$ (mA/cm^2)	$I_{p,c}$ (mA/cm^2)	I_{pa}/ I_{pc}
TONTs-N_2	0.474	0.098	0.38	4.6	- 4.2	1.12
TONTs-N_2/10mM W dopant	0.757	0.501	0.26	3.4	- 4.2	0.81
TONTs-N_2/10mM V dopant	0.447	0.098	0.35	4.7	- 4.1	1.14
TONTs-N_2 /50mM V	0.461	0.067	0.39	4.5	- 3.8	1.17
TONTs-air /10mM V dopant	1.038	- 0.580	1.62	2.4	- 2.4	1.00

3.4 Photochemical characteristics of V-doped titanium oxide nanotubes arrays and supporting electrolyte in 1M KOH.

Fig. 11: Shows the pulse chronoamperometry (CA) in 1 M KOH. The transient photocurrent response of titanium oxide nanotubes anodized for 20 min was measured under illumination with several 20 s light on/off cycles at zero bias. As shown in Fig. 11, the dark current value tends to zero. Under illumination conditions, the photocurrent rapidly rises to a constant value of 26 mA/cm^{2,} which indicates that the charge transfer process is very rapid. The pattern photocurrent is highly reproducible for several light on-off cycles. The forms of the I-t curve and V-t curve are typical of that obtained using potentiostat/galvanostat under these conditions, which are attributed to the photogene ration and recombination of electron hole pairs under light on/off conditions. Under illumination, the photo induced electrons transport from the wall of TONTs to Ti substrate rapidly to produce photocurrent. Under dark conditions, the hole recombines with electrons from TiO_2 conduction band that leads to the decrease of photocurrent.

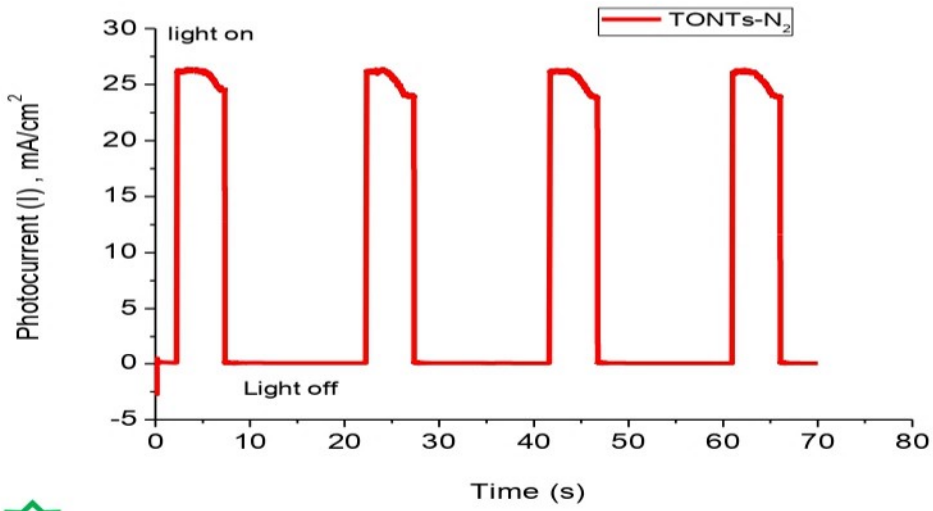

Fig. 11: The transient photocurrent response of TiO_2 nanotubes anodized in 20 V for 20 min in 0.5 wt. % HF and annealing in N_2 at 450°C for 3 h.

To further investigate the photoresponse of titanium oxide nanotubes samples anodized at 20 minutes, the dark I-V characteristics and the I-V characteristics under illumination were also carried out by linear sweep voltammetry at a scan rate of 50mV/s at an applied potential of 1.0 V vs. SCE. The dark I-V curves of TONTs samples anodized at 20 min are superposed practically. Fig 12 shows the dark current of TiO_2 NTs anodized for 20 min, and the value is around 10^{-3} mA/cm^2. Under illumination, the photocurrent density increases with the increase of applied potential and gradually reaches a plateau value at 1.0 V (vs. SCE), which indicates the applied electric field efficiently promotes the separation of photo generated charge carriers. As shown in Fig 12, anodization time has a significant effect on the photocurrent.

The photocurrent of samples first increases with increasing anodization time during 10 min-60 min with further increase in anodization time, a decrease of photocurrent is observed. The maximum photocurrent measured TiO_2 NTs anodized for 60 min. This result explains that the nanotube length of TiO_2 NTs mainly depends on the anodization time and increases with increasing anodization time.

TiO_2 NTs with longer tube length induce a larger active surface area and higher absorption of incident photons, which results in more photogenerated electron-hole pairs and enhances the photocurrent density [53]. However, due to the existence of the effective depth of light penetration [54], when the tube length exceeds a certain range, the light penetration to the under-layer is restrained which leads to the decrease of photocurrent. Most importantly, longer pathways for electron transfer to Ti substrate may provide a higher chance for charge recombination [55].

Fig. 12 shows Photocatalytic properties of Titanium oxide nanotubes arrays in UV-light and of in situ solution V-doped titanium oxide nanotubes grown by anodization in 0.5 wt. % HF and supporting electrolyte was 1 M KOH. CV and CA was under UV-light in 1 M KOH, anodization was in 0.5 wt. % HF in 20V for 20 minutes, geometric area of working electrode (TONTs arrays) was 0.68 cm^2.

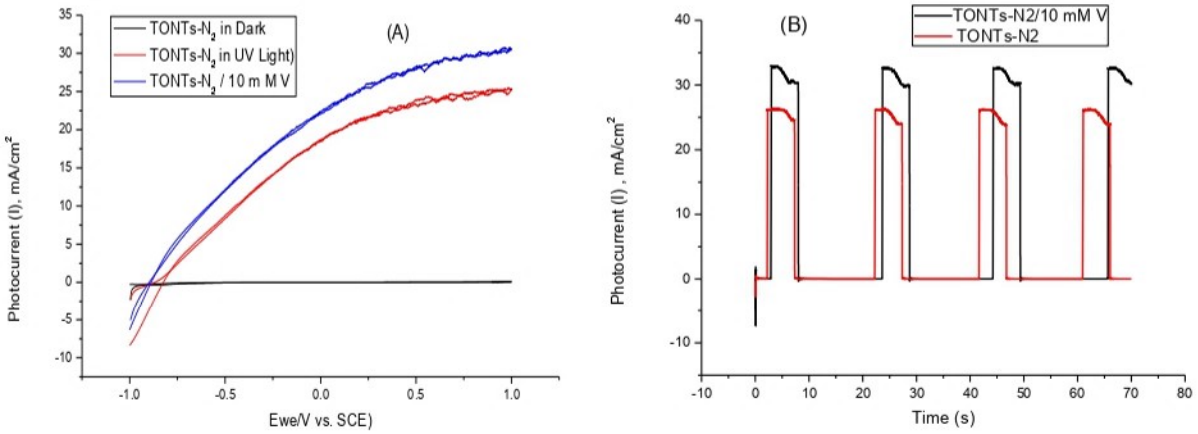

Fig. 12: Photo electrochemical properties of TONTs electrodes (A) Linear-sweep voltammograms of TONTs-N_2 in dark, TONTs-N_2 and TONTs-N_2/10 mM V dopant electrodes under illumination (UV-light) at a scan rate 50 mV/s and supporting electrolyte is 1 M KOH. (B) Corresponding amperometric **I–t** curves at an applied potential of 1.0 V vs. SCE under illumination with 60 s light on/off cycles.

TiO_2 is an effective photocatalyst [56, 57]. However, it can be only activated under UV light irradiation of wavelength < 387 nm because of its large band gap of 3.2 eV. Recently, it was reported that doping TiO_2 with non-metals such as nitrogen [56-59] , carbon [60,61], fluorine [62] and iodine [63] could induce its photocatalytic activity under visible light, which may be due to band gap narrowing [56] or the creation of surface oxygen vacancies [62,64]. Additionally, the specific surface area has a strong influence on the visible-light activity of TiO_2. Recently, highly ordered TiO_2 nanotubes with an individual tube diameter of approximately 100 nm and a tube length of approximately 500 nm have been fabricated by electrochemical anodization [65–71]. The method is based on anodization of Ti in diluted HF-containing electrolytes.

4. Conclusions

TiO_2 NTs arrays have been efficiently prepared via anodic oxidation of titanium foil in 0.5 wt. % HF at 20 V for 20 min., solution followed with annealing in air and N_2. The annealing treatment may help to form different point defects, such as oxygen vacancies, titanium forming and occupying interstices and more complex structures, which will increase the conductivity and have great effect on the properties of the electrode. Annealing in dry nitrogen at 450 °C for 3 hrs seemed to be the most favorable conditions to retain desired nanotube array structure with desirable anatase phase and electrochemical properties in $[Fe(CN)_6]^{-3/-4}$ solution. Partial reduction of tetravalent titanium cations and the formation of oxygen vacancies may attributed to clarify the modification of the electrochemical and properties of the TONTs arrays.

On the other hand, when comparing between CVs of 10mM $K_4[Fe(CN)_6] + K_3[Fe(CN)_6]$ + 0.5 M KCl TiO_2 NTs annealed in N_2 and 0.07 cm^2 glassy carbon electrodes , it was observed that the peaks anodic and cathodic current densities of titanium oxide nanotube annealing in nitrogen are close to the peaks anodic and cathodic current densities of glassy carbon electrode, while the titanium oxide nanotube annealing in air,

titanium oxide nanotube as anodized do not show any clear peaks . Therefore, they have lower conductivity and glassy carbon exhibits high electrical conductivity in contrast with other electrodes and also TONTs-N_2 show electrical conductivity close to that of glassy carbon but higher than that of TONTs-as anodized and TONTs-air electrodes. This was evidence that the TONTs-N_2 has high electroactivity but little less conductive than that of glassy carbon electrode.

Vanadium-doped TiO_2 NTs arrays show greatly enhanced electrochemical properties compared with TiO_2 nanotubes. Vanadium metal dopant is the best of all metals dopants because it gives CV with high current and low oxidation/reduction separation ΔE in comparison with other dopants, i.e. TONTs-N_2/V dopants give high surface area, high and improved conductivity and high stability similar to the N_2-dopant. In summary, vanadium-doped TiO_2 NTs arrays show greatly enhanced electrochemical properties compared with TiO_2 nanotubes. On the other hand the, N_2-dopant is the best of all dopants for metals and non-metals as electro catalyst.

It has been found that doping TiO_2 nanotubes with such nonmetals as N_2 makes it more responsive to UV.

However, the main challenge with doped TiO_2 photo catalysts remains that the photocatalytic activity under visible light is lower than that under ultra-violet light. Therefore, further development of these photo catalysts is needed. A major area of future research is the development of optimized dopants and doping strategies.

5. Acknowledgements

The authors would like to use this opportunity to express their gratitude to King Saud University, Chemistry Department.

6. Notes and references

[1] Nabil AN Alkadasi, MA Awad, MA Ghanem, AM Al-Mayouf. Palladium supported on titanium oxide nanoparticles as a catalyst for methanol oxidation reaction. International Journal Of Chemistry Studies. (2018): 2(3):10-16.

[2] A. Fujishima, K. Honda, Electrochemical photolysis of water at a semiconductor electrode, Nature238 (1972)37–38.

[3] S. Liu, A .Chen ,Coadsorption of horseradish peroxidase with thionine on TiO_2 nanotubes for biosensing,Langmuir18 (2005) 8409 – 8413.

[4] H. Li, L . Cao, W . Liu, G . Su, B . Dong, Synthesis and investigation of TiO_2 nanotube arrays prepared by anodization and their photo- catalytic activity,Ceramics International 38(2012)5791–5797.

[5] V. S. Saji, H. C. Choe, W. A . Brantley, An electrochemical study on self-ordered nanoporous and nanotubular oxide on Ti – 35Nb – 5Ta – 7Zr alloy for biomedical applications , Acta Biomaterialia 5(2009) 2303–2310.

[6] G. K . Mor, K . Shankar, M . Paulose, O . K . Varghese, C . A . Grimes, Enhanced photocleavage of water using titania nanotube arrays, Nano Letters 5 (2005) 191 – 195.

[7] K . Zhu, T . B . Vinzant, N . R . Neale, A . J. Frank,Removing structural disorder from oriented TiO_2 nanotube arrays: reducing the dimen - sionality of transport and recombination in dye-sensitized solar cells, Nano Letters7 (2007) 3739 – 3746.

[8] K. Zhu, N.R. Neale, A. Miedaner, A.J. Frank, Nano Lett. 7 (2007) 69.

[9] J.R. Jennings, A. Ghicov, L.M. Peter, P. Schmuki, A.B. Walker, J. Am. Chem. Soc.130 (2008) 13364.

[10] O.K. Varghese, D. Gong, M. Paulose, K.G. Ong, E.C. Dickey, C.A. Grimes, Adv.Mater. 15 (2003) C662.

[11] G . K . Mor, K . Shankar, M . Paulose, O . K . Varghese, C . A . Grimes, Nano. Lett. 5 (2005)191.

[12] B. O'Regan, M. Gr̈tzel, Nature 353 (1991) 737–740.

[13] L.K. Tan, K.K. Manippady, W.W. An, H. Gao, Appl. Mater. Interfaces 2 (2010) 498

[14] F. Fabregat-Santiago, E.M. Barea, J. Bisquert, G.K. Mor, K. Shankar, C.A. Grimes,J. Am. Chem. Soc. 130 (2008) 11312.

[15] K.L. Li, Z.B. Xie, S. Adams, Z. Kristallogr. 225 (2010) 173.

[16] Z.B. Xie, S. Adams, D.J. Blackwood, J. Wang, Nanotechnology 19 (2008) 405701–405711.

[17] A. Ghicov, P. Schmuki, Chem. Commun. 20 (2009) 2791.

[18] R. Asahi, T. Morikawa, T. Ohwaki, K. Aoki, Y. Taga, *Science.* 6 (2001) 293,269.

[19] M. Mrowetz, W. Balcerski, A. J. Colussi, M. R. Hoffman, *J. Phys. Chem.* 108 (2004)17269-17273.

[20] G. Sauthier, E. Gyorgy, A. Figueras. *J. Mater. Res.* 23 (2008) 2340-2345.

[21] W. Y. Su, Y. F. Zhang, Z. H. Li, L. Wu, X. X.Wang, J. Q. Li, X. Z. Fu. *Langmuir. 24 (*2008) 3422-3428.

[22] K. Iketani, R. D. Sun, M. Toki, K. Hirota, O. Yamaguchi. Mater. Sci. Eng., B 108(2004) 187-193.

[23] A .Ahmad, J. A. Shah, S. Buzby, S. I .Shah, *Eur. J. Inorg. Chem.*6 (2008) 948-953.

[24] H. Kato, A. Kudo, *J. Phys. Chem*. B 106 (2002) 5029-5034.

[25] Z. Y. Zhao, Q. J. Liu. *Catal. Lett.* 124 (2008) 111-117.

[26] R. Nakamura, T. Tanaka, Y. Nakato. J. Phys. Chem. B, 108 (2004), pp. 10617–10620.

[27] R. Asahi, T. Morikawa, T. Ohwaki, K. Aoki, Y. Taga. *Science.*293 (2001) 269-271.

[28] S. Luciane. Santos, T. C. Nilson .Oliveira, M. Lepienski Carlos, E. B. Marino. Cláudia, Neide. K. Kuromoto. *REVISTA MAT.*19 (2014) 33-39.

[29] M. Niinomi and M. Nakai. *Int. J. Biomater*, vol.2011 (2011) 836-587.

[30] S. Oh, C. Daraio, L. Chen, T. R. Pisanic, R. R. Fin, and S. Jin. *J Biomed Mater Res A.* 78 (2006) 97-103.

[31] O.K. Varghese, D. Gong, M. Paulose, C.A. Grimes, E.C. Dickey, *J. Mater. Res.* 18 (2003) 156–165.

[32] R. Beranek, H. Tsuchiya, T. Sugishima, J.M. Macak, L. Taveira, S. Fujimoto, H. Kisch, P. Schmukic, *Appl. Phys. Lett*. 87 (2005) 243114-1–2.

[33] N. Ferreira, L. Silva, E. Corat, V. Trava-Airoldi. *Diam Relat Mater*, 11 (2002) 1523e31.

[34] W. J. Lee, M. Alhoshan, W. H. Smyrl. Journal of the Electrochemical Society, 153 (2006) 499–505.

[35] Dawei Gong, Craig A.Grimes, Oomman K. Varghese , Wenchong Hu, R. S. Singh, Zhi Chen and Elizabeth C. Dickey, Journal of Materials Research 16 (2001) 3331-3334

[36] G. K . Mor, O. K . Varghese, M. Paulose, K. Shankar, C. A. Grimes. *Mater Solar Cells.* 90 (2006) 2011-2075.

[37] V.P. Parkhutik, V. I. Shershulsky. *J. Phys D:* Apple Phys., 25 (1992) 1258 -*1263*.

[38] J.M. Macak, H. Tsuchiya , A. Ghicov, K. Yasuda , R. Hahn, S. Bauer, P. Schmuki, *Current Opinion in Solid State and Materials Science*, 11 (2007) 3–18.

[39] H. Masuda, H.Yamada, M. Satoh, H. Asoh, M. Nakao, T.Tamamura, *Appl. Phys. Lett.* 71 (1997) 2770- 2772.

[40] K. Yasuda, P. Schmuki. *Electrochim Acta.* 52 (2007) 4053-4061.

[41] G. K. Mor, K. Shankar, M. Paulose, O. K. Varghese, C.A. Grimes. *Nano Letters* 5 (2005) 191–5.

[42] Peng Xiao, Dawei Liu, Betzaid Batall Garcia , Saghar Sepehri, Yunhuai Zhang, Guozhong Cao. *Sensors and Actuators B*. 134 (2008) 367–372.

[43] J. Zang, Y. Wang, L. Bian, J. Zhang, F. Meng,Y. Zhao, X. Qu, S. Ren, Bucky. *International Journal of Hydrogen Energy*, 37 (2012) 6349-6355.

[44] E.Michael. G. Lyons and Gareth P. Keeley. Sensors. 6 (2006) 1791-1826.

[45] H. Gerischer, *Electrochim. Acta*, 35(1990) 1677–1699.

[46] T. Ma, M. Akiyama, E. Abe, I. Imai. *Nano Lett.* 5 (2005) 2543–2547.

[47] J.M. Macak, B.G. Gong, M. Hueppe, P. Schmuki. *Adv. Mater.*19 (2007) 3027–3031.

[48] F. Guillemot, M.C. Porte, C. Labruge` re, Ch. Baquey. *J. Colloid Interf . Sci* . 255 (2002) 75–78.

[49] V. Vaithianathan, S. Hishita, J.H. Moon, S.S. Kim, *Thin Solid Films* .515 (2007) 6927–6930.

[50] A. Ghicov, H. Tsuchiya, J.M. Macak, P. Schmuki. *Phys. Stat. Sol.* (a) 203 (2006) R28–R30.

[51] The Merck Index, IIth Ed. (1988) 538, #3415.

[52] J. A. Stanford, J. B. Justice, Jr.96 (1996) 359A-366A.

[53] Ku Y, Fan ZR, Chou YC, Wang WY. Characterization and induced photocurrent of TiO_2 nanotube arrays fabricated by anodization. J Electrochem Soc (2010); 157(6):671-5

[54] Liang HG, LiXZ. Effects of structure of anodic TiO_2 nanotube arrays on photocatalytic activity for the degradation of 2, 3-dichlorophenol in aqueous solution. J Hazard Mater (2009); 162:1415-22.

[55] J,Wang , Lin ZQ. Dye-Sensitized TiO_2 nanostructure solar cells with markedly enhanced performance via rational surface engineering. Chem Mater (2010); 22(2):579-84.

[56] A. Fujishimax, K. Honda, Nature 238 (1972) 37.

[57] R. Asahi, T. Morikawa, T. Ohwaki, K. Aoki, Y. Taga, Science 293 (2001) 269.

[58] T. Mokawa, R. Asahi, T. Ohwaki, K. Aoki, Y. Taga, Jpn. J. Appl. Phys. 40 (2001) L561.

[59] G.R. Torres, T. Lindgren, J. Lu, C.G. Granqvist, S.E. Lindquist, J. Phys. Chem. B 108 (2004) 5995.

[60] S.U.M. Khan, M. Al-shahry Jr., W.B. Ingler, Science 297 (2002) 2243.

[61] H. Irie, Y. Watanabe, K. Hashimoto, Chem. Lett. 32 (2003) 772.

[62] D. Li, H. Haneda, S. Hishita, N. Ohashi, N.K. Labhsetwar, J. Fluorine Chem. 126 (2005) 69.

[63] X.T. Hong, Z.P. Wang, W.M. Cai, F. Lu, J. Zhang, Y.Z. Yang, N. Ma, Y.J. Liu, Chem. Mater. 17 (2005) 1548.

[64] T. Ihara, M. Miyoshi, Y. Iriyama, O. Matsumoto, S. Sugihara, Appl. Catal. B: Environ. 42 (2003) 403.

[65] V. Zwilling, M. Aucouturier, E. Darque-Ceretti, Electrochim. Acta 45 (1999) 921.

[66] D. Gong, C.A. Grimes, O.K. Verghese, Z. Chen, E.C. Dickey, J. Mater. Res. 16 (2001) 3331.

[67] C.M. Ruan, M. Paulose, O.K. Varghese, C.A. Grimes, Sol. Energy Mater. Sol. C 90 (2006) 1283.

[68] Q. Xie, S.G. Yang, X.L. Ruan, H.M. Zhao, Environ. Sci. Technol. 39 (2005) 3770.

[69] Y.K. Lai, L. Sun, C. Chen, C.G. Nie, J. Zuo, C.J. Lin, Appl. Surf. Sci. 252 (2005) 1101.

[70] R. Beranek, H. Hildebrand, P. Schmuki, Electrochem. Solid State Lett. 6 (2003) B12.

[71] J.L. Zhao, X.H. Wang, R.Z. Chen, L.T. Li, Solid State Commun. 134 (2005) 705.

تحضير دعامات حفاز وتشخيصها من مصفوفة أنابيب ثاني أوكسيد التيتانيوم النانوية غير المطعمة والمطعمة

أ. محمد أحمد حسين عوض أ.د. نبيل عبدالله القدسي

الملخص:

لقد تم تحضير دعامات حفاز من أنابيب ثاني أوكسيد التيتانيوم النانوية النشطة ذات التوصيلية الكهربائية العالية عن طريق الأكسدة المصعدية الكهروكيميائية في 0.5 **wt** % من محلول **HF** عند جهد ثابت مقداره 20 فولت، ولمدة زمنية مقدارها 20 دقيقة، ومن ثم المعالجة الحرارية في جو من النيتروجين أو الهواء.

وتم تحضير أنابيب ثاني أوكسيد التيتانيوم النانوية المعالجة حراريًا في جو من النيتروجين أو الهواء والمطعمة ببعض الفلزات، مثل الفناديوم والتنجستن، وذلك بواسطة التطعيم في المحلول أثناء عملية الأكسدة المصعدية الكهروكيميائية.

تم إجراء التوصيفات الفيزيائية اللازمة بواسطة حيود الأشعة السينية والمجهر الإلكتروني الماسح، وتم دراسة السلوك الكهروكيميائي للمواد المنتجة من أوكسيد التيتانيوم النانوي غير المطعم والمطعم ببعض الفلزات باستخدام التوصيف الكهروكيميائى بدراسة منحنيات الوقت مع كثافة التيار أثناء عملية الأكسدة المصعدية الكهروكيميائية في محلول فلوريد الهيدروجين، وبدراسة منحنيات مسح الجهد الدوري في محلول سداسي سيانيد الحديد.

وكذلك تم دراسة السلوك الكيميائي الضوئي للمواد المنتجة من أوكسيد التيتانيوم النانوي غير المطعم والمطعم بالفناديوم في محلول قاعدي من هيدروكسيد البوتاسيوم .

كلمات مفتاحية:

صفيحة أنابيب ثاني أوكسيد التيتانيوم النانوي، تقنية الأكسدة المصعدية الكهروكيميائية، الفناديوم، التنجستن، التطعيم الكيميائي، المجهاد الدوري، منحنيات الوقت مع التيار.